

Hybrid optimization tuned deep neural network-based wind power generation system for permanent magnet synchronous generator control

Prashant Kumar S. Chinamalli, Mungamuri Sasikala

Department of Electrical and Electronics Engineering, Shambasva University, Kalaburagi, India

Article Info

Article history:

Received Oct 19, 2024

Revised Dec 21, 2024

Accepted Jan 16, 2025

Keywords:

Coati optimization

Deep neural network optimization

Loss minimization

Lyrebird optimization

Permanent magnet synchronous generator

Wind power generation

ABSTRACT

Wind energy, a cost-effective renewable source, has seen substantial growth. permanent magnet synchronous generator (PMSG) equipped wind turbines demonstrate superior performance in variable-speed applications. However, there remains a notable research gap in optimizing the overall system efficiency for such wind energy systems. Therefore, this research presents to develop a deep learning-based optimization technique that improves the efficiency of PMSG-based wind energy systems by minimizing overall system losses and maximizing energy output. Core loss and rotor speed data were fed into a deep neural network for various operating conditions ranging from 50 to 1000 rpm, to determine optimal system parameters. This work introduces a hybrid lyrebird-based coati optimization algorithm (LB-COA) to optimize the deep neural networks (DNN) classifier, combining two advanced optimization techniques to improve model performance. Simulation results validate that the proposed optimization strategy efficiently boosts the system's dynamic performance and overall power efficiency.

This is an open access article under the [CC BY-SA](https://creativecommons.org/licenses/by-sa/4.0/) license.



Corresponding Author:

Prashant Kumar S. Chinamalli

Department of Electrical and Electronics Engineering, Shambasva University

Kalaburagi, India

Email: prashantvnc@gmail.com

1. INTRODUCTION

The escalating global demand for sustainable energy alternatives to fossil fuels has driven significant interest in wind energy technology [1]. Its compelling attributes, such as cost-effectiveness, ease of installation, and minimal maintenance requirements, have contributed to its rapid growth in recent years [2], [3]. Permanent magnet synchronous generators (PMSG) based wind energy conversion systems (WECS) have gained substantial popularity because of their compact size, high output power, and higher torque-to-inertia ratio. Unlike doubly-fed induction generator (DFIG) systems, PMSGs feature a simpler internal structure without the need for complex gearboxes or brushes. These advantages have positioned PMSG-based WECS as a focal point of research and development in the wind energy sector [4]. The fluctuating and erratic nature of wind speed poses a substantial challenge to maximizing the output of high-power wind generators. Consequently, these systems often operate below their full potential, hindering the overall effectiveness of wind energy utilization and diminishing the anticipated aids of large-scale wind power generation. The intermittent nature of wind speed poses significant challenges for grid integration of large-scale wind farms. Fluctuations in wind energy output can introduce instability into the power system. Wind turbines, complex machines influenced by various meteorological factors, further complicate the integration process. Wind energy conversion is affected by various factors, such as wind speed, blade pitch angle, and rotor speed. Moreover, the intermittent nature of wind and energy losses within the WECS pose significant challenges to

system stability [5]. Therefore, WECS is a complex process categorized by substantial fluctuations and concerns. To address these challenges, researchers have explored numerous control strategies and theories for PMSG systems over the past few decades [6].

Because of their uncomplicated design, reliability, and straightforward implementation, proportional integral (PI) controllers remain a popular choice for enhancing the stability of both the grid side converter (GSC) and rotor side converter (RSC) in PMSG-based wind turbines. Reference employs a proportional integral (PI) controller to enhance PMSG wind turbine performance under both steady and fluctuating wind conditions [7]. Nevertheless, the linear nature of PI control limits its adaptability to the nonlinear dynamics of the PMSG system, as well as its resilience to variation in wind and turbine conditions. To address power quality challenges in wind turbine systems, various nonlinear control strategies have emerged. Notable examples include fuzzy logic controller (FLC), backstepping control, and direct power control (DPC) [8], [9]. Fuzzy control, despite its potential for high accuracy, is problematic to implement due to its reliance on substantial expert input and subjective human interpretation, often leading to delayed responses. While DPC offers superior transient performance, it requires high switching frequencies to mitigate torque and current ripple, as reported in [10].

Meta-heuristic algorithms have been successfully employed to address intricate engineering challenges [11]. For instance, genetic algorithm (GA) has been utilized to optimize PI controller parameters for PMSG during grid disturbances [12]. Moreover, particle swarm optimization (PSO) has been applied to PMSG systems operating under varying wind speeds, while firefly algorithm (FA) has been used to enhance maximum power point tracking (MPPT) performance through pitch angle control of PMSG [13], [14]. For instance, combined an adaptive ant colony optimization (AACO) algorithm with a general regression neural network (GRNN) to improve MPPT [15]. Additionally, the whale optimization algorithm has been applied to optimize machine-side converter parameters for MPPT [16]. Collectively, these studies demonstrate the potential for optimization algorithms in improving both MPPT and low voltage ride through (LVRT) capabilities of PMSG-driven wind energy systems by tuning either the machine-side converter (MSC) or grid side converter (GSC) parameters [17]. Population-based metaheuristic algorithms, such as the lyrebird optimization algorithm (LOA), offer several advantages over traditional optimization techniques. LOA's ability to balance exploration and exploitation enables it to find optimal solutions in a relatively short time, making it suitable for PMSG-based wind power generation. The subsequent section highlights the key contributions:

- a. Proposes a deep neural networks (DNN) model that helps to minimize the discrepancy between actual and predicted data using error metrics. This model aims to enhance the accuracy of predictions by reducing the error between the observed and estimated values.
- b. Introduced a hybrid lyrebird-coati optimization algorithm (LB-COA) to optimize DNN classifier weights, thereby improving the performance, prediction accuracy, and energy efficiency of wind power generation using PMSGs.
- c. The novel integration of deep learning with hybrid optimization techniques addresses key challenges in PMSG-based WECS.
- d. Comparative analysis reveals that the suggested model surpasses traditional counterparts in generating output power, minimizing losses, and enhancing efficiency.

The structure of this paper is as follows: section 2 presents a thorough review of existing literature. Section 3 presents a detailed model of the PMSG-based wind turbine system. The LB-COA technique for parameter tuning is elaborated in section 4. The performance evaluation and results are discussed in section 5, and the paper concludes with a summary of key findings in section 6.

2. LITERATURE REVIEW

2.1. Related works

A novel control strategy combining fuzzy field-oriented control (FFOC) with direct power control (DPC) for variable speed wind energy conversion systems (VSWECS) was proposed in [18]. This method aims to improve system performance by enhancing energy extraction and minimizing losses through the optimization of turbine operation parameters. Stability, robustness, performance, and balanced current injection are all enhanced by the combined control algorithm. An innovative optimization technique for PMSG-based wind turbines was presented in study [19]. Their approach prioritized maximizing WEG while concurrently decreasing the overall system losses. To achieve optimal wind power output, the proposed method focused on optimizing torque per ampere (TPA), as well as quadrature current. The objective function, which is impacted by both d-q axis current, is core loss minimization. The performance of the suggested aquila with African vulture optimization (EA-AVO) is evaluated by comparing its output power, losses, efficacy, and convergence speed with established approaches. A pioneering control strategy to

optimize interior permanent-magnet synchronous generator (IPMSG)-based systems was introduced in [19]. Their method employed polynomial parameters to curtail IPMSG losses and amplify WECS. This study presents an innovative hybrid optimization technique named crossover assisted whale optimization algorithm (CWOA), which effectively determines optimal coefficients for maximizing power generation. This framework optimizes tip speed ratio, considered a critical parameter for wind energy conversion. It also accounts for the nonlinear behavior of the IPMSG due to magnetic saturation. To assess the efficacy of the CWOA algorithm, it is compared against established techniques like WOA, firefly algorithm (FF), artificial bee colony (ABC), and genetic algorithm (GA).

A novel sliding mode control (SMC) strategy for PMSG in wind energy conversion systems, with a focus on maximizing power output, was introduced in study [20]. SMC's robustness in handling nonlinear electrical systems has made it a popular choice in this domain. This research employs a nonlinear PMSG model to implement SMC control. The primary goal is to regulate stator PQ power, as well as voltage frequency, for optimal grid integration. The results demonstrate enhanced system robustness. A comprehensive model of a variable-speed wind turbine equipped with a PMSG was presented in study [21]. Their control strategy aimed to optimize wind power capture by employing field-oriented control (FOC) and an ideal speed setpoint determined by wind conditions. A comparative analysis of PSO and its variants was conducted to optimize PI controller gains at convergence. The results indicated that the PSO-based controller exhibited inferior performance metrics across various error criteria when compared to the explicitly defined controller. A novel sensorless technique capable of operating PMSGs across a wide speed range was developed in [22]. This technique leverages the current controller's output within the speed control loop. This study introduced an opposition particle swarm optimization-support vector regression (OPSO-SVR) algorithm for wind speed prediction using historical offline data. The proposed approach addresses the challenge of support vector regression (SVR) parameter optimization across a broad wind speed spectrum. Employing OPSO yields faster and more accurate optimal SVR parameters. The developed algorithm excels at rapid and precise wind speed estimation through swift optimization and tuning of SVR parameters. It accurately tracks real wind speed values and is sovereign of generator turbine constants or torque measurements. Thus, the experimental findings confirm outstanding performance in predicting wind speed and rotor speed.

Ant lion optimizer (ALO) was proposed to tune the parameters of a conventional PI controller for a wind energy system with a PMSG [23]. Their aim was MPPT while enhancing fault ride-through performance. The proposed method effectively enhanced low voltage ride through (LVRT) performance while maximizing power extraction. The findings demonstrate a substantial enhancement in overall system dynamics when contrasted with the traditional PI controller. An advanced MPPT strategy coupled with pitch angle control was introduced in [24]. This research focuses on two primary objectives. The first is to coordinate the generator and GSC to follow the optimal wind speed setpoint determined by the MPPT technique. The second is to mitigate the chattering issue inherent in standard SMC by introducing a novel smooth continuous SMC strategy. Furthermore, Lyapunov stability analysis validates the proposed sliding mode controller. Simulation results underscore the controller's effectiveness in achieving precise, stable operation with minimal output current ripple.

2.2. Review

Table 1 provides an overview of several controlling methods for PMSG-based WECS. Initially, a DNN classifier, which can handle unstructured and unlabeled data, was recommended in [25]. However, overfitting remains a significant challenge encountered in this approach. Furthermore, the AI-AVO method, designed to prevent premature convergence and achieve optimal solutions, faces challenges such as slow convergence rates, high computational demands, and sensitivity to parameter settings [19]. Likewise, the CWOA strategy, presented to decrease parameter optimization time, still requires significant computational resources to determine optimal parameters [20]. Additionally, SMC control, proposed for enhanced system performance and high robustness, encounters the challenge of the chattering phenomenon [21], [25]. Similarly, the PI+PSO scheme, introduced, is easy to implement and converges faster but is computationally expensive [22]. In addition, the OPSO-SVR model suggested, which offers better performance and faster convergence, is computationally intensive and requires careful parameter tuning for optimal results [23]. The ALO-PI strategy, developed, offers superior performance and eliminates the need for gradient information; however, a major drawback is its slow convergence and is computationally expensive [24]. Therefore, this research endeavors to resolve the previously outlined issues and optimize WECS performance through PMSG integration.

Table 1. Features and challenges of PMSG-based WECS using various controlling strategies

Author [citation]	Methodology utilized	Features	Challenges
Salime <i>et al.</i> [18]	FFOC	<ul style="list-style-type: none"> – Power quality with low harmonic distortion – Simple implementation 	<ul style="list-style-type: none"> – Face challenges especially in systems with faster dynamics or under extreme load conditions
Chinamalli and Sasikala [19]	AI-AVO approach	<ul style="list-style-type: none"> – Prevents premature convergence and achieves optimal solutions 	<ul style="list-style-type: none"> – However, they also face challenges in terms of slow convergence rates, high computational demands and sensitive parameter settings
Chinamalli and Sasikala [20]	CWOA technique	<ul style="list-style-type: none"> – Decrease parameter optimization time 	<ul style="list-style-type: none"> – Determining optimal parameters can be computationally demanding
Laabidine <i>et al.</i> [21]	SMC control	<ul style="list-style-type: none"> – Offers high levels of robustness for enhanced system performance 	<ul style="list-style-type: none"> – A significant challenge associated with SMC is the chattering phenomenon
Hannachi <i>et al.</i> [22]	PI+PSO	<ul style="list-style-type: none"> – Easy to implement – Converges faster 	<ul style="list-style-type: none"> – Computationally expensive
Abo-Khalil <i>et al.</i> [23]	OPSO-SVR model	<ul style="list-style-type: none"> – Better performance – Converges quickly 	<ul style="list-style-type: none"> – However, it is computationally intensive and requires careful parameter tuning for optimal performance.
Haridy <i>et al.</i> [24]	ALO-PI strategy	<ul style="list-style-type: none"> – Offers superior performance – Eliminates the need for gradient information. 	<ul style="list-style-type: none"> – Converges slowly – Computationally expensive
Majout <i>et al.</i> [25]	PSMC control	<ul style="list-style-type: none"> – Offers high levels of robustness for enhanced system performance 	<ul style="list-style-type: none"> – A significant challenge associated with SMC is the chattering phenomenon

3. SYSTEM MODEL OF A PMSG-BASED WIND TURBINE GENERATION SYSTEM

By employing a permanent magnet to transform the mechanical energy generated by the wind turbine into AC electricity, the IPMSG acts as a generator. The generator transforms the mechanical rotation into electrical energy by use of magnetic fields. A generator's electric output may rise with an increase in load current or rotor speed. An insulated-gate bipolar transistor (IGBT)-based pulse width modulation (PWM) converter is then used to rectify this AC output into DC power, which is then sent into a DC link. A PWM converter is used to modify the AC output voltages of the IPMSG in order to control its power output. With the aid of an additional energy inverter, this enables the IPMSG to deliver AC power into the grid or a load while preserving its steady voltage and frequency. Whereas A_d defines the air density; B_r implies the area swept in the rotor blade which is $B_r = \pi r_w^2$; Let the rotor radius be r_w in meters, v states the WT velocity and C_w characterizes the wind power factor which is a function of tip speed ratio (α) and the blade pitch angle (δ) [26]. While ω_r demonstrate the wind rotating speed in rad/sec. The mechanical output power of wind is,

$$P_o = \frac{1}{2} A_d B_r v^3 C_w(\alpha, \delta) \quad (1)$$

$$C_w = 0.5(\alpha - 0.022\delta^2 - 5.6)e^{-0.17\alpha} \quad (2)$$

$$\alpha = \frac{r_w N_s}{v} \quad (3)$$

3.1. Modelling of IPMSG

The developed IPMSG modeling system, which takes into consideration both copper loss and core loss in the stator, is shown in Figure 1. Moreover, core loss attributed to hysteresis and eddy current losses are represented by an equivalent core-loss resistance R_{cl} . Additionally, a process is developed to compute the value of R_{cl} , which varies linearly with IPMSG rotor speed ω_{Rotor} according to the model in [27].

$$R_{cl} = J_r * \omega_{Rotor} \quad (4)$$

where, $J_r = 0.2083$ (Ω/rpm).

By using permanent magnets to create the rotor's magnetic field, a PMSG is a synchronous generator that does not require an external DC field. This technology offers several advantages, making PMSG a preferred choice for various applications. The brushless and slip ring-free design of the PMSG enables a compact size, high reliability, and reduced mechanical friction losses. Its power density, or energy output per unit volume, is optimized. Additionally, the PMSGs are more efficient because they do not require rotor power conversion or a loss, which increases the generator's total efficiency [27]. Additionally, PMSGs have a greater working range, which enables them to function better in low wind speed situations when other generator types can have trouble. Because PMSGs do not depend on power electronics or slip rings for

control, they also have better grid compatibility, which lowers maintenance costs and boosts system dependability [28].

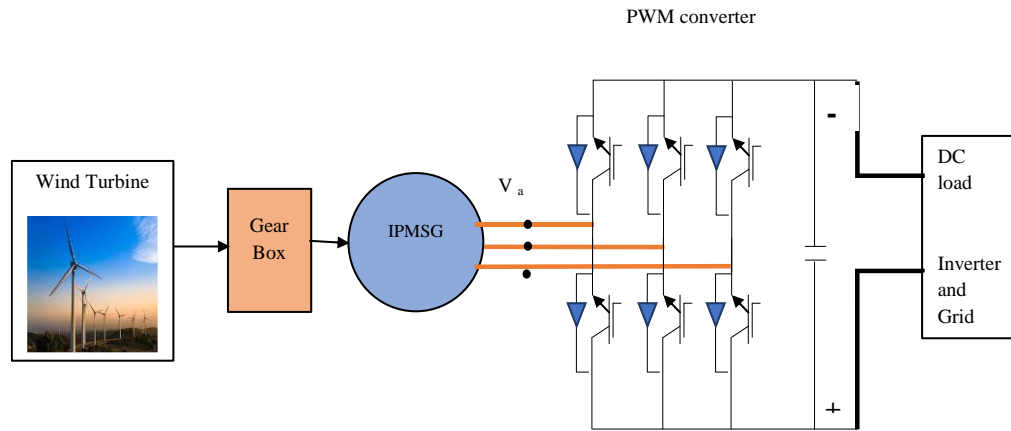


Figure 1. IPMSG system model

The PMSG model developed in this study is based on several simplifying assumptions commonly employed to reduce model complexity [29], [30]. First of all, a key assumption is the absence of magnetic circuit saturation. Secondly, neglecting eddy current losses and hysteresis linearizes the flux-current relationship. Additionally, a sinusoidal magnetomotive force (MMF) distribution is assumed. Given the smooth pole design, rotor damping is considered minimal. The PMSG stator voltage equations are expressed in the d-q synchronous reference frame [31].

$$v_d = r_x I_{dx} - h_d \frac{dI_{dx}}{dt} + \omega_s h_{qx} I_{qx} \tag{5}$$

$$v_q = r_x I_{qx} - h_q \frac{dI_{qx}}{dt} + \omega_x h_{dx} I_{dx} + \omega_x \phi_l \tag{6}$$

here, ϕ_l defines the flux linkage of PM; v_d and v_q states the d-q voltages of the stator; I_{dx}, I_{qx} implies the d-q current of the stator; h_{dx}, h_{qx} depicts the inductance of d-q axis. Magnetic saturation can be incorporated into the analysis by modeling h_q in terms of I_q . While w defines a positive constant integer, the nonlinearity introduced by the IPMSG system's susceptibility to magnetic saturation limits the applicability of loss minimization methods and linear control theory. To overcome this constraint, the study employs a nonlinear control strategy. The expression for the electromagnetic torque is given by (7), (8),

$$h_q = h_{qx} - w |I_q| \tag{7}$$

$$T_{EM} = -\frac{3}{4} n_s [\phi_l i_{qx} + (h_d - h_q) I_{dx} I_{qx}] \tag{8}$$

3.2. Maximizing wind turbine output

To maximize energy output E_o , the wind turbine's rotational speed is carefully controlled. Across a range of wind speeds, the system can maximize its efficiency by maintaining the ideal tip speed ratio α . This yields high mechanical output energy from the wind turbine. As indicated by (9), the ideal IPMSG rotor speed is directly proportional to wind speed, with the constant d_w constrained by wind turbine limitations [32].

$$\omega_{r0} = d_w v_w \tag{9}$$

3.3. Copper and core loss reduction in IPMSG

There are four types of PMSG losses: mechanical, stray-load, core, and stator copper. Of these, stator current fundamentals directly affect and control only stator copper and core losses. Consequently, this paper determines the IPMSG's maximum efficiency point through an offline nonlinear optimization process aimed at minimizing combined copper and core losses. whereas, $\phi_l = 0.246$; $r_x = 0.1764$, I_{dc} signifies the

overall I_d signals, I_q defines the optimal value with a lower bound of -50 and higher bound of 10. ρ symbolizes the best value with a higher limit of 30 and lower limit of 6. r_x and R_{cl} be the stator resistance and core-loss resistance. Moreover, V states the viscous damping coefficient in Kg square metre/s; T_{MECH} indicates the input mechanical torque. Whereas, h_{CPR} and h_C states the copper as well as core losses [30]. I_{MAX} and V_{MAX} implies the maximal IPMSG current and voltages. Minimal loss,

$$h_{loss} = h_{CPR} + h_C \quad (10)$$

Subjected to

$$h_{CPR} = 1.5r_x(I_d^2 + I_q^2) \quad (11)$$

$$I_d = -v^{-1}(PI_{dc}^2 + QI_{dc}^3 + RI_{dc}^4 - S) \quad (12)$$

$$v = \phi_l r^3 \rho + \omega_s^2 - 2I_{qc}^2 \gamma^2 \phi_l V_d^4 \tau \rho \omega_s^2 (r_x + R_{cl}) \quad (13)$$

$$R_{cl} = l_r * \omega_G = (0.2083/60) * (1200/60) \quad (14)$$

$$\omega_s = \frac{n_s * \omega_G}{2} = \frac{6 * (1200/60)}{2} \quad (15)$$

$$\gamma = \frac{h_q}{h_d} = \frac{20.5822 * 10^{-3}}{6.24 * 10^{-3}} \quad (16)$$

$$P = 3 \left((\omega_s^2 * h_d^2 * (r_x + R_{CL}) * \phi_l^2 * \tau) + (1 + \tau) * (h_d \phi^2 \tau \alpha) - ((2 * I_q^2 * \gamma^2 * \phi_l * h_d^5 * \tau^3 * \alpha * \omega_s^2)(r_s + R_{CL})) \right) \quad (17)$$

$$Q = \left((3 * h_d^2 * \phi_l * \tau^2 * \alpha) + (3 * \omega_s^2 * h_d^4 * \tau^2) \right) / (r_x + R_{CL}) * \phi_l (1 + \tau) \quad (18)$$

$$R = (h_d^2 * \tau^3 * \alpha) + (h_d^5 * \tau^3 * \omega_s^2)(r_x + R_{CL}) \quad (19)$$

$$S = -(I_q^2 * \phi_l^2 * \gamma^2 * h_d^3 * \alpha * \omega_s^2 * \tau) \quad (20)$$

$$h_C = 1.5(I_{dc}^2 + I_{qc}^2)R_{CL}(\omega_G) \quad (21)$$

$$= 1.5\omega_s^2 \left[(h_d I_{dx} + \phi_l)^2 + (h_q(I_q)I_{qx})^2 \right] / R_{CL}(\omega_G) \quad (22)$$

From (1)-(3), (7) and (8)

$$v_d = r_x I_d - \omega_s h_d (I_q) I_{qx} \quad (23)$$

$$v_q = r_x I_q + \omega_s h_d I_{dx} + \omega_s \phi_l \quad (24)$$

$$I_{dx} = I_d - (v_d - r_x I_d) / R_{CL}(\omega_G) \quad (25)$$

$$I_{qx} = I_q - (v_q - r_x I_q) / R_{CL}(\omega_G) \quad (26)$$

$$T_{MECH} - T_{EM} - V\omega_G = 0 \quad (27)$$

$$T_{MECH} = P_0 / \omega_G \quad (28)$$

$$\omega_s = n_s \omega_G / 2 \quad (29)$$

$$I_d^2 + I_q^2 \leq i_{MAX}^2 \quad (30)$$

$$v_d^2 + v_q^2 \leq v_{MAX}^2 \tag{31}$$

3.4. Dataset collection

Following the data collection methodology outlined in paper, this study employs two datasets corresponding to rotor speeds of 50 and 100 rpm [33]. The primary focus is to analyze the core losses associated with these rotor speeds, along with determining optimal parameters. To achieve this, key metrics such as quadrature current I_q' and tip speed ratio α' were carefully recorded for a range of rotor speeds, providing a comprehensive understanding of performance dynamics.

3.5. Data pre-processing

Data normalization is a preprocessing technique that transforms numerical features into a common scale. This process is essential to provide features with higher values from dominating calculations. By standardizing the data, we reduce bias towards particular variables by standardizing the data, guaranteeing that each characteristic contributes fairly to the analysis. Data normalization is a critical preprocessing step in the development of robust DNN. Extensive research has highlighted its role in enhancing model accuracy. A widely employed normalization method is min-max scaling, which linearly transforms data to a specified range, typically between 0 and 1 [33]. Whereas, $Norm$ simulates the normalization signal and N indicates the collection of signals across all charging cycles.

$$Norm = \frac{N - N_{MIN}}{N_{MAX} - N_{MIN}} \tag{32}$$

3.6. Deep neural network

A DNN architecture comprises an input layer, followed by one or more hidden layers, and culminating in an output layer as depicted in Figure 2(a)[34]. Each layer contains interconnected nodes, forming a hierarchical structure. Information propagates forward through these layers, generating the predicted target values at the output layer as in Figure 2(b). As shown in (33) and (34) outline the mathematical computation of the target value based on input variables. Here, X_1 and X_2 represent input features, while N_1 and N_2 denote hidden layer node values. The activation function F transforms these values. The final output or predicted value is represented by \hat{Y} , which is influenced by weights (W) and biases (B) applied throughout the network. The weighted sum of the inputs is converted into a non-linear output via the activation function. A commonly employed activation function in regression models is the Rectified Linear Unit (ReLU) [35]. A threshold of zero is applied by the non-linear activation function ReLU. If the input (Z) is negative, it returns zero. Otherwise, it returns the input value unchanged.

$$\begin{cases} N_1 = F(X_1W_{11} + X_2W_{21} + B_1) \\ N_2 = F(X_1W_{12} + X_2W_{22} + B_2) \end{cases} \tag{33}$$

$$\hat{Y} = F(N_1W_{31} + N_2W_{32} + B_3) \tag{34}$$

$$F = \begin{cases} Z < 0 & F(Z) = 0 \\ Z \geq 0 & F(Z) = Z \end{cases} \tag{35}$$

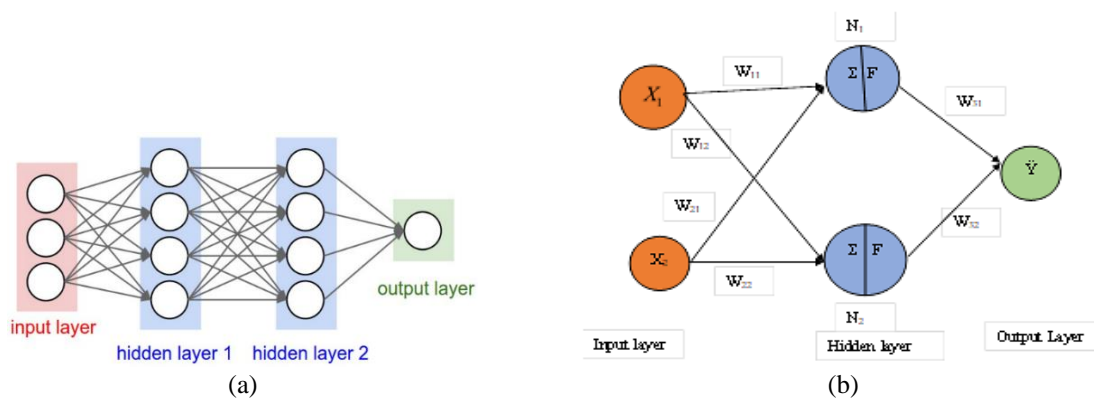


Figure 2. Overview of the DNN model and its output (a) structure of the DNN model and (b) predicted output of the DNN

To enhance model accuracy, the backpropagation algorithm iteratively adjusts layer weights by minimizing the discrepancy between predicted and actual values [36]. This optimization process involves calculating the error function's gradient using gradient descent, subsequently updating neuron weights to reduce the overall error. The proposed methodology utilizes core loss and rotor speed as input parameters for a DNN model, while the corresponding tip speed ratio ' α ' and quadrature current ' I_q ' are designated as target outputs. To optimize the model's performance and maximize wind power generation, the hybrid Lyrebird-based coati optimization (LB-COA) algorithm is employed to refine relevant model parameters.

4. PARAMETER TUNING VIA HYBRID LB-COA ALGORITHM

4.1. Objective function

The study aimed to optimize PMSG-based WECS by integrating deep learning and optimization algorithms. The weights of the DNN classifier are optimally tuned using a proposed hybrid LB-COA. This algorithm serves as the objective function, ensuring that the solution bounds remain within the range of 0 to 1. By leveraging this proposed LB-COA approach, the study aims to enhance the accuracy and efficiency of the DNN classifier, demonstrating the effectiveness of the LB-COA in optimizing complex neural network parameters. The effectiveness of the optimization was evaluated through simulations comparing the system's performance with the existing models like DNN-PMSG, lyrebird optimization algorithm + deep neural networks (LOA+DNN), coati optimization algorithm + deep neural networks (COA+DNN), sand cat swarm optimization + deep neural networks (SCSO+DNN), and zebra optimization algorithm + deep neural networks (ZOA+DNN) [34], [37]–[40].

4.2. Developed hybrid LB-COA technique

LOA [37] is a population-based metaheuristic technique employing a population of artificial lyrebirds. The Lyrebird optimization algorithm (LOA) can be applied to various types of optimization problems, particularly those involving complex, high-dimensional, and nonlinear objective functions. Each lyrebird represents a potential solution, characterized by its position within the problem domain. Each lyrebird's behavior can be modelled as a point in decision space. The hybrid LB-COA is an advanced modification of the basic LOA method. It combines the principles of the LOA with another optimization technique, coati optimization algorithm (COA), to enhance performance. While the basic LOA is effective for searching global optima, it may struggle with local convergence in certain complex optimization problems. By integrating COA, the LB-COA hybrid improves the exploration and exploitation balance.

4.3. LOA statistical model

The developed LOA technique dynamically adjusts population member positions at each iteration by simulating the lyrebird's behavior in response to perceived threats. Inspired by the lyrebird's behavior, the population update involves two primary actions: escaping and hiding. Figure 3 denotes the flowchart of LB-COA approach.

The LOA algorithm simulates the lyrebird's strategic choice between fleeing and hiding when faced with danger, modeled by (36). Consequently, each LOA position is adjusted in each iteration depending on one of the two phases. Where, Rnd defines the arbitrary count within the range [0,1].

Update process for

$$H_p: \begin{cases} asperStage1, Rnd \leq 0.5 \\ asperStage2, else \end{cases} \quad (36)$$

Stage 1: strategy for escaping (explored level)

During this LOA level, population members are repositioned within the searching space by mimicking the lyrebird's escape from a perilous location to safer grounds. Significant positional alterations are caused by this dynamic movement, which improves the algorithm's ability to search globally by enabling it to investigate various areas of the solution space. People choose population members with higher objective function values as preferred target locations in the LOA framework. These identified positions constitute the safe area set for each member, calculated using (37).

$$S_p = \{H_k, Of_k < Of_p \text{ and } k \in \{1, 2, \dots, n\}\} \quad (37)$$

while, $p = 1, 2, \dots, n$. At this time, S_p defines the safest area set for p^{th} lyrebird; H_k implies the H matrix with k^{th} row with an objective function of Of_k which is better than the p^{th} LOA member. The LOA

algorithm simulates a random escape of the lyrebird to one of the identified safe areas. A new location for each population member is computed depending on this simulated displacement according to (38). If the new position yields an improved objective function value, it changes the earlier position according to (39).

$$H_{p,q}^{L1} = H_{p,q} + Rnd_{p,q} \cdot (SA_{p,q} - B_{p,q} * H_{p,q}) \tag{38}$$

$$H_p = \begin{cases} H_p^{L1}, & Of_p^{L1} \leq Of_p \\ H_p, & \text{else,} \end{cases} \tag{39}$$

In this context, SA_p denotes the chosen safe area for the i^{th} lyrebird, with $SA_{p,q}$ representing its p^{th} dimensional coordinate. H_p^{L1} states the newly computed location of the p^{th} lyrebird according to the proposed LOA's escape mechanism. Of_p^{L1} calculates the objective functional value, $Rnd_{p,q}$ represent the arbitrary count among 0 and 1, while $B_{p,q}$ defines the randomly assigned values of either 1 or 2.

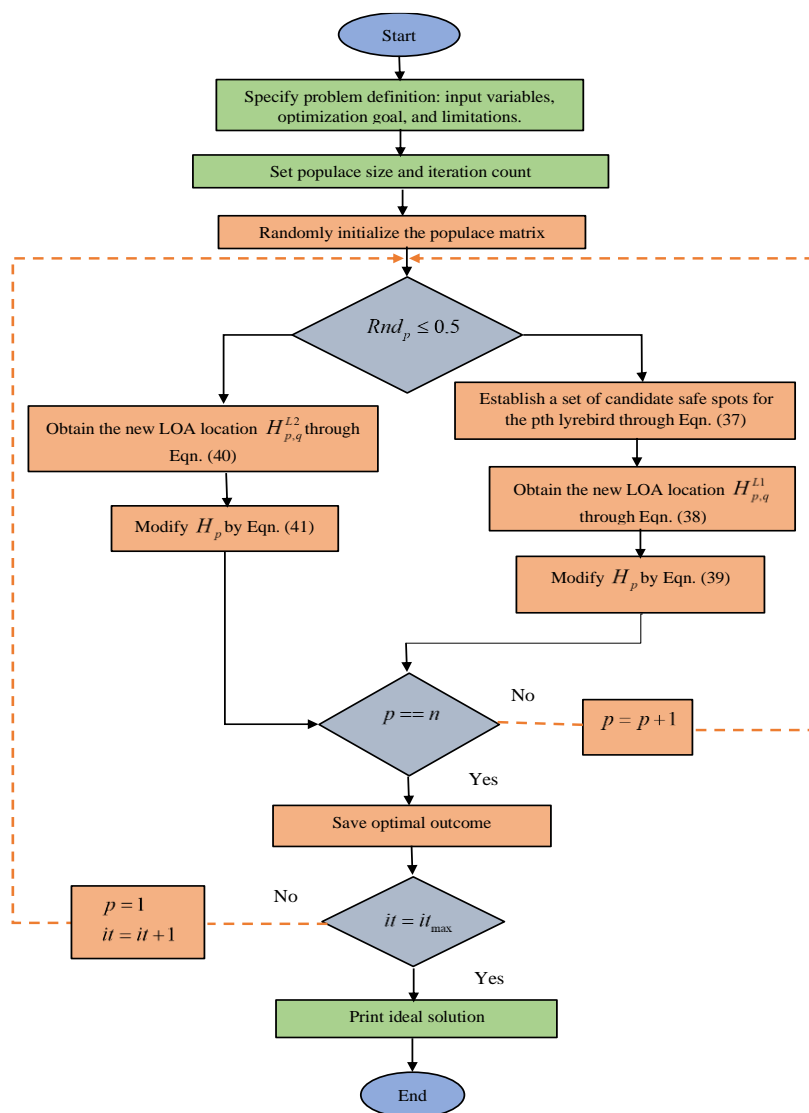


Figure 3. Flowchart of LB-COA technique

Stage 2: strategy for hiding (exploited level)

This LOA phase emulates the lyrebird's strategy of concealing itself within its immediate safe zone. By meticulously examining the surrounding environment and making incremental movements towards a

suitable hiding spot, the algorithm refines its position subtly. The behavior of the process of escaping from predators are same for both LOA and coati optimization (i.e.,) exploitation phase. Therefore, coati [38] is best suited for escaping through social behavior, climbing and defensive aggression. It can leverage its social structure for increased vigilance and can quickly move to a safe place if threatened. So based on the above strategy the exploitation phase equation of coati is used in the LOA technique named as lyrebird optimization algorithm-based coati optimization (LB-COA) algorithm.

$$H_{p,q}^{L2} = H_{p,q} + (1 - 2Rnd) \cdot (LB_q^{local} + Rnd \cdot (UB_q^{local} - LB_q^{local})) \quad (40)$$

while,

$$\begin{aligned} LB_q^{local} &= LB_q / it \\ UB_q^{local} &= UB_q / it \\ H_p &= \begin{cases} H_p^{L2}, & Of_p^{L2} \leq Of_p \\ H_p, & \text{else,} \end{cases} \end{aligned} \quad (41)$$

while, H_p^{L2} indicate the current location depending on the LOA hiding strategy. The objective function value Of_p^{L2} is assessed for this new position. Rnd states the arbitrarily chosen bound within [0,1] and it be the iteration count. Algorithm 1 depicts the pseudocode of the presented LB-COA strategy.

Algorithm 1. Pseudocode of LB-COA

```

Provide problem definition: input variables,
optimization goal, and limitations.
Set npopulace size and iterations (it)
Randomly initialize the populace matrix
     $H_{p,d} \leftarrow LB_d + Rnd \cdot (UB_d - LB_d)$ 
Calculate the fitness
Ascertain the most suitable option
For  $it = 1$  to  $it_{max}$ 
    For  $P = 1$  to  $n$ 
        Identify the lyrebird's defensive tactic against
        predation utilizing Eqn. (36)
        If  $Rnd_p \leq 0.5$  (Stage 1)
            Establish a set of candidate safe spots for the  $p^{th}$ 
            lyrebird through Eqn. (37)
            Obtain the new LOA location through Eqn. (38)
            Modify the LOA member's position by Eqn. (39)
        else (Stage 2)
            Obtain the new LOA location through Eqn. (40)
            Modify the LOA member's position by Eqn. (41)
        end if
    end while
end (For  $P = 1$  to  $n$ )
Save the optimal outcome
end (For  $it = 1$  to  $it_{max}$ )
Output the optimal result within LOA
end LOA

```

5. RESULTS AND DISCUSSIONS

5.1. Experimental setup

A Simulink model, as seen in Figure 4, was used to produce data for managing a PMSG-based WEGS constructed in the MATLAB 2021b environment in order to evaluate the efficacy of the suggested LB-COA DNN technique. A performance comparison was conducted between the obtained results and those of alternative approaches such as DNN-PMSG, LOA+DNN, COA+DNN, SCSO+DNN, and ZOA+DNN [34], [37]–[40]. To highlight the efficiency of the suggested control method, the dynamic behavior and steady-state of the WTG system is examined in this section for learning rates of 70%, 80%, and 90%. A thorough evaluation of the model's performance was displayed utilizing a range of error metrics, such as “mean absolute error (MAE), mean squared error (MSE), root mean squared error (RMSE), mean absolute percentage error (MAPE), mean absolute relative error (MARE), mean squared relative error (MSRE), and root mean squared relative error (RMSRE),” which confirmed its accuracy. In addition, the convergence graph and the computational time have also been analyzed in comparison with the traditional models.

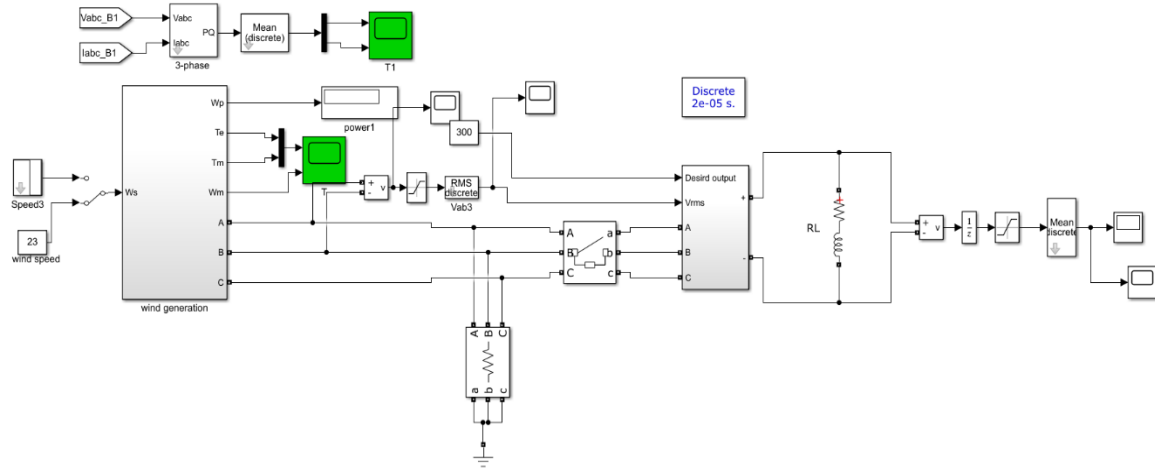


Figure 4. Simulation setup

Figures 5(a) to 5(e) display a visual comparison of real-time data versus predicted data waveform for the existing COA, LOA, SCSO, and ZOA methods and LB-COA+DNN method, focusing on sample size and target values with a 70% learning rate. On observing the result, it can be noted that the predicted value of the adopted LB-COA+DNN model is very close to the actual data when compared to existing COA, LOA, SCSO, and ZOA methods. This improved performance indicates that the proposed model is more efficient in modelling the underlying data patterns, leading to predictions that closely align with actual values. Likewise, Figures 6(a) to 6(e) and Figures 7(a) to 7(e) present the waveform of actual versus predicted data for the LB-COA+DNN model over traditional COA, LOA, SCSO, and ZOA models under learning rates of 80% and 90%, respectively. According to the findings, combining the LB-COA method with deep neural networks improves the model's capacity for data learning and increases its dependability for real-world uses. These results demonstrate the potential benefits of the LB-COA+DNN approach over conventional techniques with regard to prediction efficacy and accuracy.

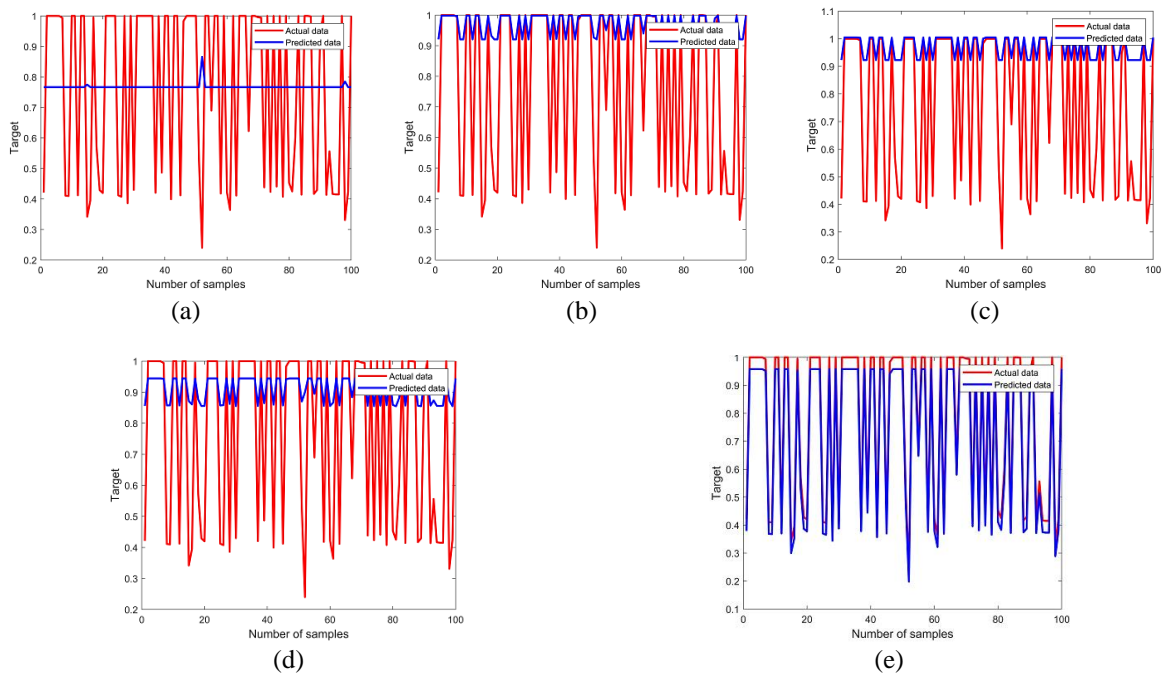


Figure 5. Waveform of actual vs predicted data for proposed over standard models under 70% learning rate, (a) COA, (b) ZOA, (c) LOA, (d) SCSO, and (e) proposed

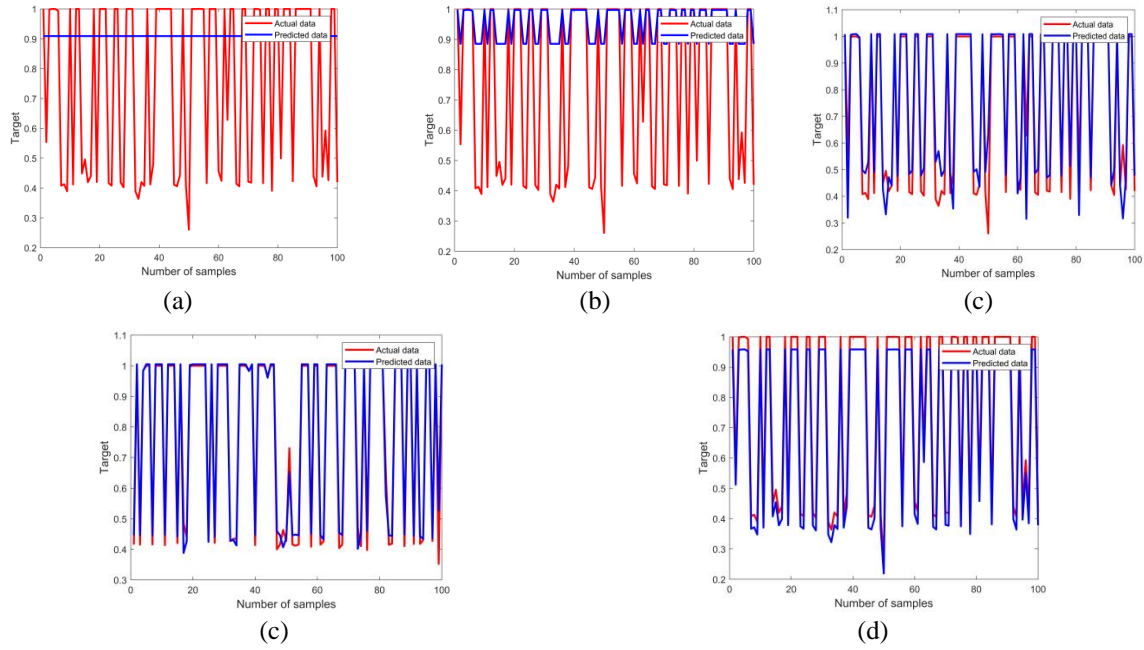


Figure 6. Waveform of actual vs predicted data for proposed over standard models under 80% learning rate, (a) COA, (b) ZOA, (c) LOA, (d) SCSO, and (e) proposed

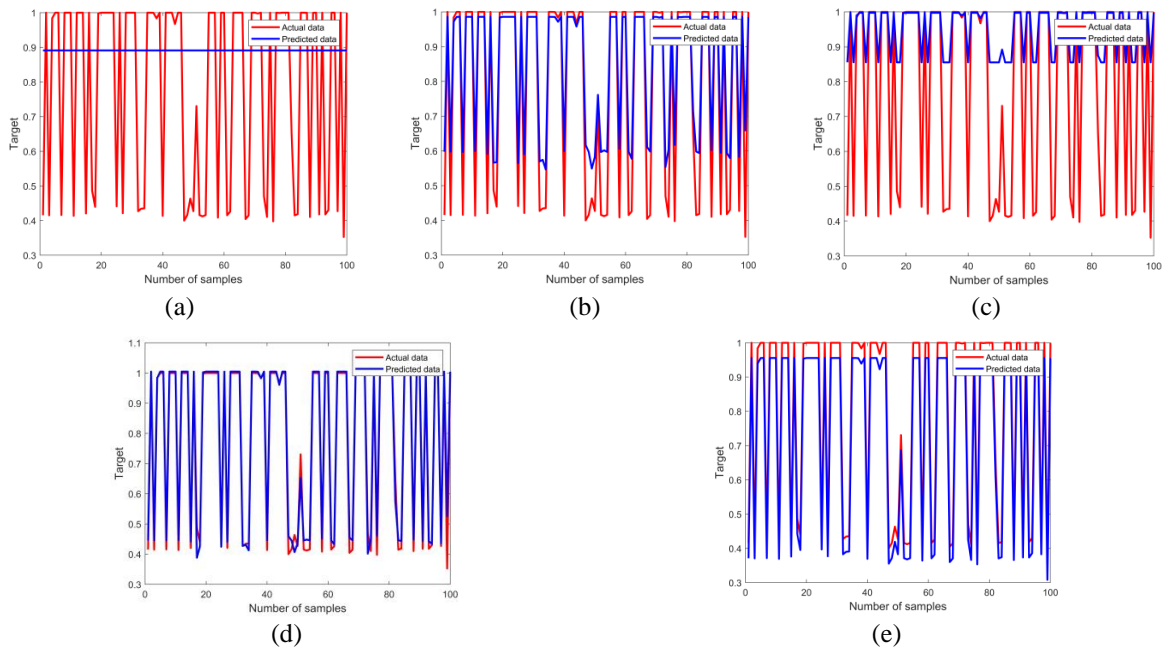


Figure 7. Waveform of actual vs predicted data for proposed over standard models under 90% learning rate, (a) COA, (b) ZOA, (c) LOA, (d) SCSO and (e) proposed

5.2. Error metrics

To evaluate the LB-COA+DNN approach, we benchmarked it against prevailing methods. As shown in Figure 8(a), the integrated LB-COA+DNN classifier significantly outperformed existing techniques by achieving a lower MAE. With a 70% LP rating, the designed LB-COA+DNN reached an MAE of 0.0420, which is superior to DNN-PMSG, SCSO+DNN, ZOA+DNN, COA+DNN, and LOA+DNN by 46.5%, 69.5%, 63.4%, 73.18%, and 63.72%, respectively. The recommended LB-COA+DNN model demonstrated superior forecasting accuracy compared to existing approaches. Notably, the LB-COA+DNN model achieved improvements of 91.79%, 96.07%, 96.69%, 95.77%, and 96.71% over DNN-PMSG, SCSO+DNN,

ZOA+DNN, COA+DNN, and LOA+DNN, correspondingly. At a learning rate of 90%, the suggested LB-COA+DNN classifier in Figure 8(b), yields a MAPE of 7.922, showing improvements of 68.89%, 43.96%, 31.17%, 72.58%, and 66.96% over the traditional DNN-PMSG, SCSO+DNN, ZOA+DNN, COA+DNN, and LOA+DNN methods, respectively. Moreover, Figure 8(c) shows that the LB-COA-DNN method attains a MARE of 0.0764528, significantly lower than the other methods like DNN-PMSG, SCSO+DNN, ZOA+DNN, COA+DNN, and LOA+DNN methods at 70% LP rating. Furthermore, the designed LB-COA+DNN model exhibited superior performance across various error metrics in which “RMSE, MAPE, MARE, MSRE, and RMSRE” values were recorded as 0.042, 7.645, 0.076, 0.067, and 0.26. In addition, the model accomplished a lower MSE of 0.0017 at an 80% LP rating, surpassing DNN-PMSG, SCSO+DNN, ZOA+DNN, COA+DNN, and LOA+DNN by 96.33%, 95.62%, 96.32%, 96.79%, and 58.87%, respectively.

The Figure 8(d) shows a significantly lower MSE of 0.0017, which outperforms competing methods by substantial margins. At 70% LP rating Figure 8(e), the LB-COA-DNN method has an MSRE of 0.0679726, the lowest among the compared techniques, while other methods have much higher values. Likewise, as shown in Figure 8(f), the proposed method at 80% rating achieves a smaller RMSE of 0.041, while the classical methods reached improvements of 80.84%, 79.07%, 80.80%, 82.11%, and 35.87% over the standard DNN-PMSG, SCSO+DNN, ZOA+DNN, COA+DNN, and LOA+DNN models, congruently. Additionally, the Figure 8(g) shows the adopted model at 90% rating achieves a smaller RMSRE of 0.08325, while the traditional methods attained improvements of 36.84%, 12.1%, 19.45%, 46.71%, and 42.6% over the traditional DNN-PMSG, SCSO+DNN, ZOA+DNN, COA+DNN, and LOA+DNN models. This study found that the LB-COA+DNN classifier outperformed better with less error rates. For a thorough assessment, Tables 2, 3, and 4 provide a comprehensive breakdown of error metrics for the proposed approach versus the existing techniques at 70%, 80%, and 90% LP rates.

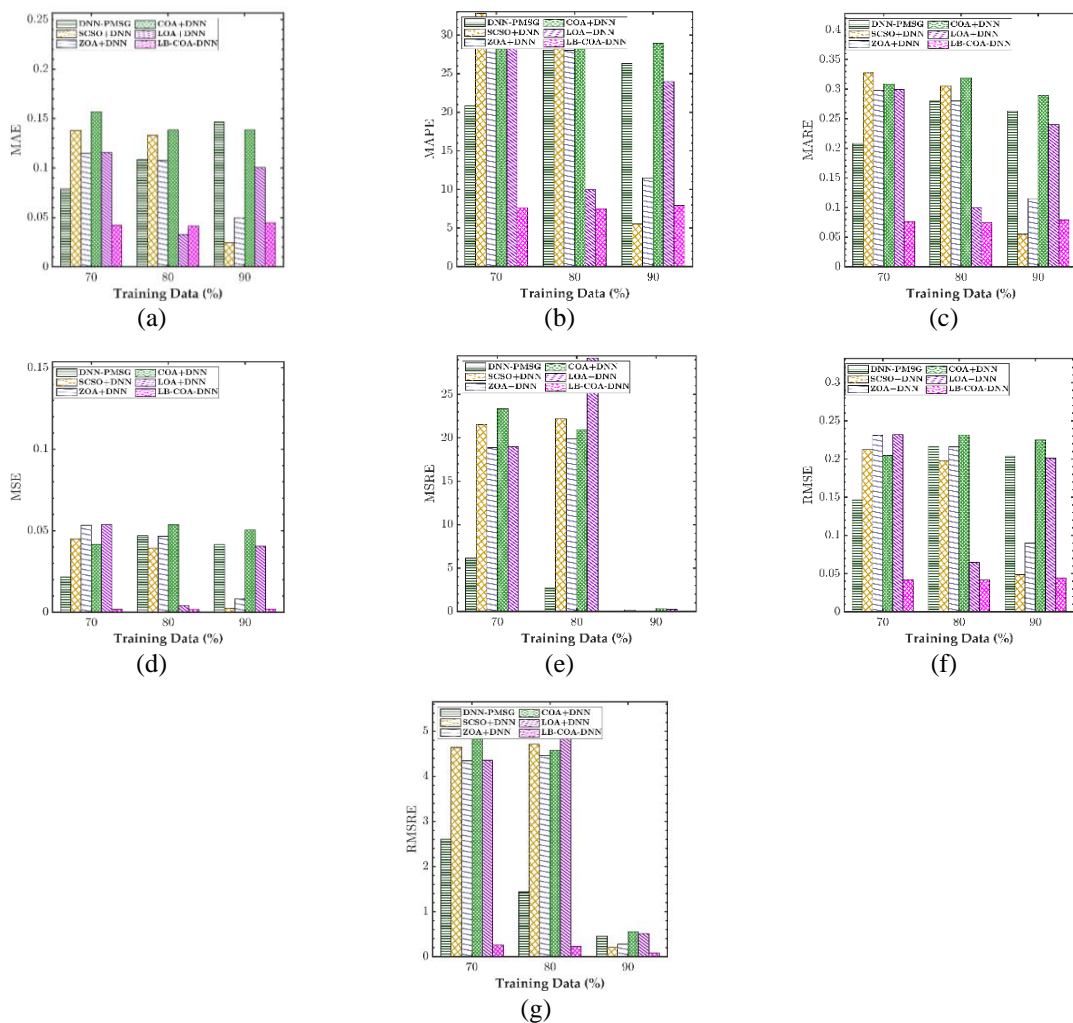


Figure 8. Error metrics of the developed over traditional techniques(a) MAE, (b) MAPE, (c) MARE, (d) MSE, (e) MSRE, (f) RMSE, and (g) RMSRE

Table 2. Comparison of error metrics for the developed technique at LP=70Row

Row	DNN-PMSG	SCSO+DNN	ZOA+DNN	COA+DNN	LOA+DNN	LB-COA-DNN
MSE	0.0215246	0.0450374	0.0534403	0.0418626	0.0537362	0.0017672
MAE	0.0788029	0.1378910	0.1147761	0.1567432	0.1158881	0.0420377
RMSE	0.1467127	0.2122201	0.2311716	0.2046035	0.2318107	0.0420377
MAPE	20.8307533	32.7897911	29.7556152	30.8906689	29.9307137	7.6452844
MARE	0.2083000	0.3278869	0.2975559	0.3089060	0.2992980	0.0764528
MSRE	6.1552181	21.5384274	18.8794765	23.3392258	18.9700050	0.0679726
RMSRE	2.5994802	4.6409512	4.3450518	4.8310690	4.3554568	0.2607156

Table 3. Comparison of error metrics for the developed technique at LP=80

Row	DNN-PMSG	SCSO+DNN	ZOA+DNN	COA+DNN	LOA+DNN	LB-COA-DNN
MSE	0.046820	0.039235	0.046612	0.053655	0.004176	0.001717
MAE	0.108249	0.133094	0.108052	0.138463	0.032662	0.041441
RMSE	0.216379	0.198079	0.215897	0.231635	0.064621	0.041441
MAPE	28.061081	30.591116	28.010122	31.920084	10.027295	7.513789
MARE	0.280619	0.305915	0.280104	0.319211	0.100274	0.075138
MSRE	2.674721	22.197403	19.854713	20.947365	29.199278	0.051107
RMSRE	1.435619	4.711412	4.455863	4.576829	5.403636	0.226068

Table 4. Comparison of error metrics for the developed technique at LP=90

Row	DNN-PMSG	SCSO+DNN	ZOA+DNN	COA+DNN	LOA+DNN	LB-COA-DNN
MSE	0.041591	0.002357	0.008055	0.050503	0.040529	0.001973
MAE	0.146884	0.024655	0.049611	0.138616	0.100682	0.044420
RMSE	0.203938	0.048545	0.089750	0.224728	0.201318	0.044420
MAPE	26.316729	5.503065	11.511068	28.901457	23.977884	7.922265
MARE	0.263167	0.055031	0.115111	0.289014	0.239778	0.079223
MSRE	0.204021	0.041722	0.077162	0.302880	0.259279	0.006930
RMSRE	0.451687	0.204261	0.277780	0.550346	0.509195	0.083245

5.3. Convergence graph

The proposed technique's fitness function assessment is shown in Figure 9, where the number of iterations is adjusted from 0 to 50. The graph reveals that our model effectively minimizes the fitness compared to other classical methods. Primarily, Figure 9(a) represents the 70% learning rate in which the fitness of the suggested system for the 10th iteration is 0.045, which is 4.25%, 2.17%, 2.82% and 6.25% better than the SCSO, ZOA, COA, and LOA techniques. In addition, the fitness function of the model consistently declines with each iteration, as visualized in the graph. Based on Figure 9(b), for an 80% learning rate, the selected LB-COA approach achieved a minimal fitness function of 0.041 for the 40th iteration which is better than SCSO by 4.4%, ZOA by 2.4%, COA by 2.56% and LOA by 2.43%, respectively. Similarly, Figure 9(c) depicts the fitness function of a 90% learning rate in which the developed LB-COA technique achieves a faster convergence at the 50th iteration, which is equal to 0.038, which is 3.5%, 0.4%, 1.3% and 2.04% superior to SCSO, ZOA, COA and LOA techniques correspondingly. The results demonstrate that LB-COA outperforms traditional approaches by significantly reducing the fitness function value. The proposed LB-COA's convergence analysis over the popular SCSO, ZOA, COA, and LOA models are shown in Table 5.

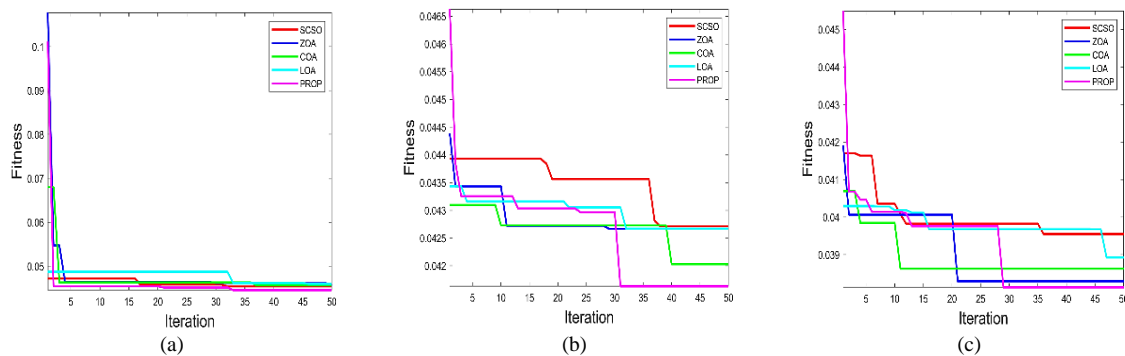


Figure 9. Convergence graph based on several LP rates, (a) LP=70, (b) LP=80, and (c) LP=90

5.4. Computational time

Table 5 provides a detailed comparison of computational times between the proposed developed LB-COA and several traditional optimization algorithms, including SCSO, ZOA, COA, and LOA. When the LP is 70, LB-COA significantly outperforms the other algorithms, achieving a computational time of 1982.4 s. The attained computational time significantly outperforms SCSO by 20172 s, ZOA by 21602 s, COA by 24656 s, and LOA by 99743 s. Similar improvements were observed for LP=80 and 90, while the developed LB-COA attains 2850.6 s and 4997.9 s when compared to the other methods.

Table 5. Computational time analysis

	SCSO	ZOA	COA	LOA	PROP
LP=70	20172	21602	24656	99743	1982.4
LP=80	26031	23758	19651	15796	2850.6
LP=90	16468	33238	16472	16267	4997.9

6. CONCLUSION

This research presented a hybrid LB-COA approach to optimize the weights of the DNN classifier, enhancing the performance, prediction accuracy, and energy efficiency of wind power generation using PMSGs. The proposed model achieved an MAE of 0.0420 after 70% training, outperforming DNN-PMSG, SCSO+DNN, ZOA+DNN, COA+DNN, and LOA+DNN by 46.5%, 69.5%, 63.4%, 73.18%, and 63.72%, respectively. Similarly, the developed LB-COA algorithm demonstrates rapid convergence, achieving a fitness value of 0.038 within 50 iterations. This represents a 3.5%, 0.4%, 1.3%, and 2.04% improvement over SCSO, ZOA, COA, and LOA, respectively, confirming the superiority of LB-COA in minimizing the fitness function. To assess the efficacy of the proposed LB-COA+DNN approach, its performance was measured against existing techniques. The LB-COA's capabilities were rigorously verified through simulations conducted in MATLAB/Simulink under diverse wind circumstances. Simulation results and comparative studies validate the evaluation of the recommended control strategy for PMSG-integrated variable-speed WECS. This hybrid optimization approach could also be used in industries involving complex systems and predictive models, such as in smart grids, electric vehicles, and robotics, where energy efficiency and accurate prediction are critical. A limitation of this research is that it does not address the challenges of implementing these optimizations in real-world, large-scale systems with varying grid conditions. Future research on PMSG control for wind energy systems will focus on optimizing efficiency, reliability, and grid integration. By leveraging advanced optimization techniques and emerging technologies, the potential to enhance WECS is immense.

FUNDING INFORMATION

Authors state no funding involved.

AUTHOR CONTRIBUTIONS STATEMENT

Prashant Kumar S. Chinamalli conceived the idea, developed the theory, and performed the analysis. Mungamuri Sasikala made a substantial contribution to the concept and design of the article. Prashant Kumar S. Chinamalli and Mungamuri Sasikala drafted the article, contributed important intellectual content, and approved the final version for publication. Prashant Kumar S. Chinamalli verified the analytical methods. Mungamuri Sasikala encouraged the investigation and supervised the findings of this work.

Name of Author	C	M	So	Va	Fo	I	R	D	O	E	Vi	Su	P	Fu
Prashant Kumar S. Chinamalli	✓	✓	✓		✓	✓		✓	✓	✓	✓		✓	
Mungamuri Sasikala	✓	✓		✓			✓		✓			✓	✓	✓

C : Conceptualization

M : Methodology

So : Software

Va : Validation

Fo : Formal analysis

I : Investigation

R : Resources

D : Data Curation

O : Writing - Original Draft

E : Writing - Review & Editing

Vi : Visualization

Su : Supervision

P : Project administration

Fu : Funding acquisition

Conflict of interest statement

Authors state no conflict of interest.

ETHICAL APPROVAL

The conducted research is not related to either human or animal use.

DATA AVAILABILITY

Derived data supporting the findings of this study are available from the corresponding author PKSC on request.

REFERENCES

- [1] B. Bossoufi *et al.*, “dSPACE-based implementation for observer backstepping power control of DFIG wind turbine,” *IET Electric Power Applications*, vol. 14, no. 12, pp. 2395–2403, Sep. 2020, doi: 10.1049/iet-epa.2020.0364.
- [2] E. M. Youness *et al.*, “Implementation and validation of backstepping control for PMSG wind turbine using dSPACE controller board,” *Energy Reports*, vol. 5, pp. 807–821, Nov. 2019, doi: 10.1016/j.egy.2019.06.015.
- [3] C. M. Hong, C. H. Chen, and C. S. Tu, “Maximum power point tracking-based control algorithm for PMSG wind generation system without mechanical sensors,” *Energy Conversion and Management*, vol. 69, pp. 58–67, 2013, doi: 10.1016/j.enconman.2012.12.012.
- [4] A. Benamor, M. T. Benchouia, K. Srairi, and M. E. H. Benbouzid, “A novel rooted tree optimization apply in the high order sliding mode control using super-twisting algorithm based on DTC scheme for DFIG,” *International Journal of Electrical Power and Energy Systems*, vol. 108, pp. 293–302, Jun. 2019, doi: 10.1016/j.ijepes.2019.01.009.
- [5] L. Pan and C. Shao, “Wind energy conversion systems analysis of PMSG on offshore wind turbine using improved SMC and Extended State Observer,” *Renewable Energy*, vol. 161, pp. 149–161, 2020, doi: 10.1016/j.renene.2020.06.057.
- [6] N. Bounar, S. Labdai, and A. Boukroune, “PSO–GSA based fuzzy sliding mode controller for DFIG-based wind turbine,” *ISA Transactions*, vol. 85, pp. 177–188, Feb. 2019, doi: 10.1016/j.isatra.2018.10.020.
- [7] J. Liu, F. Zhou, C. Zhao, Z. Wang, and B. Aguirre-Hernandez, “A PI-type sliding mode controller design for PMSG-based wind turbine,” *Complexity*, vol. 2019, no. 1, Jan. 2019, doi: 10.1155/2019/2538206.
- [8] M. A. Soliman, H. M. Hasanien, H. Z. Azazi, E. E. El-Kholy, and S. A. Mahmoud, “An adaptive fuzzy logic control strategy for performance enhancement of a grid-connected PMSG-Based wind turbine,” *IEEE Transactions on Industrial Informatics*, vol. 15, no. 6, pp. 3163–3173, Jun. 2019, doi: 10.1109/TII.2018.2875922.
- [9] M. Beniysa, A. El Janati El Idrissi, A. Bouajaj, M. Réda Britel, and E. Ariwa, “Neural network adaptive backstepping control via uncertainty compensation for PMSG-based variable-speed wind turbine: controller design and stability analysis,” *Wind Engineering*, vol. 46, no. 2, pp. 439–458, Jul. 2022, doi: 10.1177/0309524X211031269.
- [10] I. Matraji, A. Al-Durra, and R. Errouissi, “Design and experimental validation of enhanced adaptive second-order SMC for PMSG-based wind energy conversion system,” *International Journal of Electrical Power and Energy Systems*, vol. 103, pp. 21–30, 2018, doi: 10.1016/j.ijepes.2018.05.022.
- [11] B. Xing and W.-J. Gao, “Innovative computational intelligence: A rough guide to 134 clever algorithms,” *Intelligent Systems Reference Library*, vol. 62, pp. 123–137, 2014.
- [12] H. M. Hasanien and S. M. Mueyeen, “Design optimization of controller parameters used in variable speed wind energy conversion system by genetic algorithms,” *IEEE Transactions on Sustainable Energy*, vol. 3, no. 2, pp. 200–208, Apr. 2012, doi: 10.1109/TSTE.2012.2182784.
- [13] C. M. Hong, F. S. Cheng, and C. H. Chen, “Optimal control for variable-speed wind generation systems using general regression neural network,” *International Journal of Electrical Power and Energy Systems*, vol. 60, pp. 14–23, Sep. 2014, doi: 10.1016/j.ijepes.2014.02.015.
- [14] Y. S. Kim, I. Y. Chung, and S. Il Moon, “Tuning of the PI controller parameters of a PMSG wind turbine to improve control performance under various wind speeds,” *Energies*, vol. 8, no. 2, pp. 1406–1425, 2015, doi: 10.3390/en8021406.
- [15] Rukslin, M. Haddin, and A. Suprajitno, “Pitch angle controller design on the wind turbine with permanent magnet synchronous generator (PMSG) base on firefly algorithms (FA),” in *Proceedings - 2016 International Seminar on Application of Technology for Information and Communication, ISEMANTIC 2016*, 2017, pp. 13–17. doi: 10.1109/ISEMANTIC.2016.7873802.
- [16] A. A. Mohamed, A. L. Haridy, and A. M. Hemeida, “The whale optimization algorithm-based controller for PMSG wind energy generation system,” in *Proceedings of 2019 International Conference on Innovative Trends in Computer Engineering, ITCE 2019*, Feb. 2019, pp. 438–443. doi: 10.1109/ITCE.2019.8646353.
- [17] M. Rahimi, “Modeling, control and stability analysis of grid connected PMSG based wind turbine assisted with diode rectifier and boost converter,” *International Journal of Electrical Power and Energy Systems*, vol. 93, pp. 84–96, 2017, doi: 10.1016/j.ijepes.2017.05.019.
- [18] H. Salime, B. Bossoufi, S. Motahhir, and Y. El Mourabit, “A novel combined FFOC-DPC control for wind turbine based on the permanent magnet synchronous generator,” *Energy Reports*, vol. 9, pp. 3204–3221, Dec. 2023, doi: 10.1016/j.egy.2023.02.012.
- [19] P. K. S. Chinamalli and M. Sasikala, “A novel AI-AVO approach for maximum power generation of PMSG,” *Indonesian Journal of Electrical Engineering and Computer Science (IJECS)*, vol. 36, no. 1, pp. 99–114, 2024, doi: 10.11591/ijeecs.v36.i1.pp99-114.
- [20] P. S. Chinamalli and M. Sasikala, “CWOA-PMSG: Crossover assisted WOA optimization for controlling PMSG in wind generation system,” in *3rd International Conference on Electrical, Electronics, Communication, Computer Technologies and Optimization Techniques, ICECCOT 2018*, 2018, pp. 654–664. doi: 10.1109/ICECCOT43722.2018.9001403.
- [21] N. Z. Laabidine, A. Errarhout, C. El Bakkali, K. Mohammed, and B. Bossoufi, “Sliding mode control design of wind power generation system based on permanent magnet synchronous generator,” *International Journal of Power Electronics and Drive Systems (IJPEDS)*, vol. 12, no. 1, pp. 393–403, Mar. 2021, doi: 10.11591/ijpeds.v12.i1.pp393-403.
- [22] M. Hannachi, O. Elbeji, M. Benhamed, and L. Sbata, “Optimal tuning of proportional–integral controller using particle swarm optimization algorithm for control of permanent magnet synchronous generator based wind turbine with tip speed ratio for maximum power point tracking,” *Wind Engineering*, vol. 45, no. 2, pp. 400–412, Feb. 2021, doi: 10.1177/0309524X20903745.

- [23] A. G. Abo-Khalil, A. M. Eltamaly, R. P. Praveen, A. S. Alghamdi, and I. Tlili, "A sensorless wind speed and rotor position control of PMSG in wind power generation systems," *Sustainability (Switzerland)*, vol. 12, no. 20, pp. 1–19, 2020, doi: 10.3390/su12208481.
- [24] A. L. Haridy, A. A. Ali M. Abdelbasset, A. M. Hemeida, and Z. M. Ali Elhalwany, "Optimum controller design using the ant lion optimizer for PMSG driven by wind energy," *Journal of Electrical Engineering and Technology*, vol. 16, no. 1, pp. 367–380, Nov. 2021, doi: 10.1007/s42835-020-00585-5.
- [25] B. Majout *et al.*, "Improvement of PMSG-based wind energy conversion system using developed sliding mode control," *Energies*, vol. 15, no. 5, p. 1625, Feb. 2022, doi: 10.3390/en15051625.
- [26] P. M. Anderson and A. Bose, "Stability simulation of wind turbine systems," *IEEE Transactions on Power Apparatus and Systems*, vol. PAS-102, no. 12, pp. 3791–3795, 1983, doi: 10.1109/TPAS.1983.317873.
- [27] N. Urasaki, T. Senjyu, and K. Uezato, "A novel calculation method for iron loss resistance suitable in modeling permanent-magnet synchronous motors," *IEEE Transactions on Energy Conversion*, vol. 18, no. 1, pp. 41–47, Mar. 2003, doi: 10.1109/TEC.2002.808329.
- [28] A. G. Abo-Khalil and M. Alobaid, "Optimized control for PMSG wind turbine systems under unbalanced and distorted grid voltage scenarios," *Sustainability (Switzerland)*, vol. 15, no. 12, p. 9552, Jun. 2023, doi: 10.3390/su15129552.
- [29] S. Morimoto, H. Nakayama, M. Sanada, and Y. Takeda, "Sensorless output maximization control for variable-speed wind generation system using IPMSG," *IEEE Transactions on Industry Applications*, vol. 41, no. 1, pp. 60–67, Jan. 2005, doi: 10.1109/TIA.2004.841159.
- [30] S. Morimoto, M. Sanada, and Y. Takeda, "Effects and compensation of magnetic saturation in flux-weakening controlled permanent magnet synchronous motor drives," *IEEE Transactions on Industry Applications*, vol. 30, no. 6, pp. 1632–1637, Nov. 1994, doi: 10.1109/TIA.1994.350318.
- [31] J. Y. Seol and I. J. Ha, "Feedback-linearizing control of IPM motors considering magnetic saturation effect," *IEEE Transactions on Power Electronics*, vol. 20, no. 2, pp. 416–424, Mar. 2005, doi: 10.1109/TPEL.2004.842980.
- [32] W. Qiao, L. Qu, and R. G. Harley, "Control of IPM synchronous generator for maximum wind power generation considering magnetic saturation," in *Conference Record - IAS Annual Meeting (IEEE Industry Applications Society)*, Sep. 2007, pp. 1265–1272. doi: 10.1109/IAS.2007.197.
- [33] D. Singh and B. Singh, "Investigating the impact of data normalization on classification performance," *Applied Soft Computing*, vol. 97, 2020, doi: 10.1016/j.asoc.2019.105524.
- [34] J. Baek and Y. Choi, "Deep neural network for ore production and crusher utilization prediction of truck haulage system in underground mine," *Applied Sciences (Switzerland)*, vol. 9, no. 19, p. 4180, 2019, doi: 10.3390/app9194180.
- [35] X. Glorot, A. Bordes, and Y. Bengio, "Deep sparse rectifier neural networks," in *Proceedings of the 14th International Conference on Artificial Intelligence and Statistics (AISTATS)*, 2011, pp. 315–323.
- [36] D. E. Rumelhart, G. E. Hinton, and R. J. Williams, "Learning representations by back-propagating errors," *Nature*, vol. 323, no. 6088, pp. 533–536, Oct. 1986, doi: 10.1038/323533a0.
- [37] M. Dehghani, G. Bektymyssova, Z. Montazeri, G. Shaikemelev, O. P. Malik, and G. Dhiman, "Lyrebird optimization algorithm: a new bio-inspired metaheuristic algorithm for solving optimization problems," *Biomimetics*, vol. 8, no. 6, p. 507, 2023, doi: 10.3390/biomimetics8060507.
- [38] M. Dehghani, Z. Montazeri, E. Trojovská, and P. Trojovský, "Coati optimization algorithm: a new bio-inspired metaheuristic algorithm for solving optimization problems," *Knowledge-Based Systems*, vol. 259, p. 110011, Jan. 2023, doi: 10.1016/j.knosys.2022.110011.
- [39] A. Seyyedabbasi and F. Kiani, "Sand Cat swarm optimization: a nature-inspired algorithm to solve global optimization problems," *Engineering with Computers*, vol. 39, no. 4, pp. 2627–2651, Apr. 2023, doi: 10.1007/s00366-022-01604-x.
- [40] E. Trojovska, M. Dehghani, and P. Trojovsky, "Zebra optimization algorithm: a new bio-inspired optimization algorithm for solving optimization problems," *IEEE Access*, vol. 10, pp. 49445–49473, 2022, doi: 10.1109/ACCESS.2022.3172789.

BIOGRAPHIES OF AUTHORS



Prashant Kumar S. Chinamalli     born on 10th June 1987, received his B.E. degree in Electrical and Electronics Engineering department from Poojya Doddappa Appa Engineering College, Gulbarga in 2010. M. Tech in Power and Energy System from Basaveshwara Engineering College, Bagalkot in 2012. He is working as assistant professor at Department of Electrical & Electronics Engineering, Faculty of Engineering and Technology (Co-Ed), Sharnbasva University, Kalaburagi, with an experience of 11 years. His areas of interest include power system, drives and renewable energy sources. He can be contacted at email: prashantvnc@gmail.com.



Mungamuri Sasikala     born on 10th December 1962, she received her B.E. degree in electrical engineering and M.E. in Power Systems from Osmania University, Hyderabad. She is currently working as a professor in the Department of Electrical and Electronics Engineering, Faculty of Engineering and Technology for Women, Sharnbasva University, Kalaburagi, with 25 years of experience. Her areas of interest include fuzzy logic, sensors, power systems, power electronics, and drives. She can be contacted at email: sasi_mun@rediffmail.com.